TECHNICAL REPORT BRL-TR-3232

BRL

PERFORMANCE PREDICTIONS FOR THE LARGE BLAST/THERMAL SIMULATOR BASED ON EXPERIMENTAL AND COMPUTATIONAL RESULTS

STEPHEN J. SCHRAML

MAY 1991

U.S. ARMY LABORATORY COMMAND

BALLISTIC RESEARCH LABORATORY
ABERDEEN PROVING GROUND, MARYLAND

NOTICES

Destroy this report when it is no longer needed. DO NOT return it to the originator.

Additional copies of this report may be obtained from the National Technical Information Service, U.S. Department of Commerce, 5285 Port Royal Road, Springfield, VA 22161.

The findings of this report are not to be construed as an official Department of the Army position, unless so designated by other authorized documents.

The use of trade names or manufacturers' names in this report does not constitute indorsement of any commercial product.

UNCLASSIFIED

REPORT DOCUMENTATION PAGE

Form Approved
OMB No. 0704-0188

1. AGENCY USE ONLY (Leave blank)	2. REPORT DATE	3. REPORT TYPE AND DATES COVERED
	May 1991	Final, Aug 89 - Mar 91

4. TITLE AND SUBTITLE
Performance Predictions for the Large Blast/Thermal Simulator Based on Experimental and Computational Results

5. FUNDING NUMBERS
1L162120AH25

6. AUTHOR(S)
Stephen J. Schraml

7. PERFORMING ORGANIZATION NAME(S) AND ADDRESS(ES)
Director
U.S. Army Ballistic Research Laboratory
ATTN: SLCBR-TB-B
Aberdeen Proving Ground, MD 21005-5066

8. PERFORMING ORGANIZATION REPORT NUMBER

9. SPONSORING / MONITORING AGENCY NAME(S) AND ADDRESS(ES)
U.S. Army Ballistic Research Laboratory
ATTN: SLCBR-DD-T
Aberdeen Proving Ground, MD 21005-5066

10. SPONSORING / MONITORING AGENCY REPORT NUMBER
BRL-TR-3232

11. SUPPLEMENTARY NOTES

12a. DISTRIBUTION / AVAILABILITY STATEMENT
Approved for public release; distribution is unlimited.

12b. DISTRIBUTION CODE

13. ABSTRACT (Maximum 200 words)

A computational study was performed with the BRL-Q1D code to determine the expected performance characteristics of the proposed U.S. Large Blast/Thermal Simulator (LB/TS). This computational study complements an earlier experimental parametric study which was performed in the 25.4-cm shock tube located at the U.S. Army Ballistic Research Laboratory (BRL). For the experiments, the BRL 25.4-cm shock tube was configured as a 1:57 scale, axisymmetric, single-driver model of the LB/TS.

This report documents two computational parametric studies which were performed to determine the range of nuclear blast simulations available with the current LB/TS design. The first parametric study is a comparison with existing experimental data to validate the computational model and to determine the limits of its accuracy. The second parametric study used the validated computational model to predict the operating range of the LB/TS design.

14. SUBJECT TERMS
Blast; Blast Tubes; Flow Fields; Gas Dynamics; Nuclear Explosion Simulation
Nuclear Weapons; Shock Tubes; Shock Waves

15. NUMBER OF PAGES
39

16. PRICE CODE

17. SECURITY CLASSIFICATION OF REPORT	18. SECURITY CLASSIFICATION OF THIS PAGE	19. SECURITY CLASSIFICATION OF ABSTRACT	20. LIMITATION OF ABSTRACT
UNCLASSIFIED	UNCLASSIFIED	UNCLASSIFIED	UNLIMITED

INTENTIONALLY LEFT BLANK.

Acknowledgement

The author wishes to acknowledge the efforts of George Coulter of BRL, who performed all the experiments in the 1:57 scale LB/TS model. His experimental data provides the foundation for this report. Thanks also go to Richard Lottero, Richard Pearson and Gerald Bulmash for reviewing this report.

INTENTIONALLY LEFT BLANK.

Table of Contents

INTENTIONALLY LEFT BLANK.

List of Figures

INTENTIONALLY LEFT BLANK.

List of Tables

INTENTIONALLY LEFT BLANK.

I. Introduction

The U.S. Army Ballistic Research Laboratory (BRL) has been conducting research to support the design of a facility intended to subject full scale military equipment to the blast and thermal environment produced by tactical nuclear weapons. This facility, termed the Large Blast/Thermal Simulator (LB/TS) [1], is designed to produce a wide range of nuclear blast and thermal environments. Shock overpressures in the simulator can range from $2 - 35$ *psi* and simulated weapon yield can range from $1 - 600$ *kT*. The design of the LB/TS is being managed by the Army Corps of Engineers for the Defense Nuclear Agency. Construction is scheduled to begin in 1991.

The LB/TS can be thought of as a large shock tube with a complex geometry. The blast portion of a nuclear blast simulation is accomplished by releasing high pressure gas from a set of relatively small steel driver tubes into a large concrete expansion section. By adjusting the initial driver parameters of pressure, temperature and volume, a desired combination of shock overpressure and simulated weapon yield can be obtained. Baffles are used to adjust the area ratio between the driver tubes and the expansion tunnel, which also affects the blast simulation. This technique is employed to extend the facility's operating range.

When completed, the driver system of the LB/TS will consist of nine steel cylinders. Each of these cylinders will have an inside diameter of 1.83 m and will have a converging nozzle and diaphragm system at its downstream end. The flow in the simulator is initiated by simultaneously rupturing all the diaphragms. The total volume of the driver system will be a maximum of 584 m^3.

Nitrogen will be used as the driver gas. The nitrogen is to be stored in liquid form prior to a test. When needed, the liquid nitrogen will be pumped into a pebble bed heater [2] where it is evaporated and heated to the desired temperature. The heated nitrogen is then sent to the driver tubes. The current gas supply design allows for rapid filling of the driver tubes to minimize loss of heat to the uninsulated driver walls. A more conventional system based on compressors would fill the tubes much more slowly. To avoid heat loss from the gas to the driver walls with a compressor based system, the driver walls would have to be heated or insulated, neither of which proved to be practical.

The expansion section of the facility will be semi-circular with a cross-sectional area of 163 m^2 and will be composed of reinforced concrete except in the area of the test section, where it will be made of steel. With an available flow area of this size, full-scale military equipment can be tested under realistic nuclear blast and thermal conditions. If the expansion section had a smaller cross-sectional area, a such equipment could significantly block the flow which would be degrade the fidelity of the blast simulation.

The test section begins 89 m from the beginning of the expansion section and is 17.7 m long. This location of the test section is considered to be the point at which the flow from the nine driver tubes is uniform in the expansion section. A thermal radiation source will be located in the test section upstream from the target. The thermal radiation associated with a nuclear burst is simulated through the combustion of a mixture of powdered aluminum

and oxygen. The combustion products are removed from the simulator by ejectors or vents located above the thermal radiation source in the test section.

An active Rarefaction Wave Eliminator (RWE) [3] will be located at the downstream end of the expansion section. This device is used to eliminate (or minimize the effects of) expansion waves which are generated when the blast wave meets the open end of the expansion section. These unwanted expansion waves travel upstream against the subsonic flow and toward the test section. They destroy the fidelity of the simulation if they reach the test section. The RWE is termed "active" because it is continuously changing the available flow area so that the expansion waves will be eliminated for the entire decaying blast wave. A schematic diagram of the LB/TS with all its major components is shown in Figure 1.

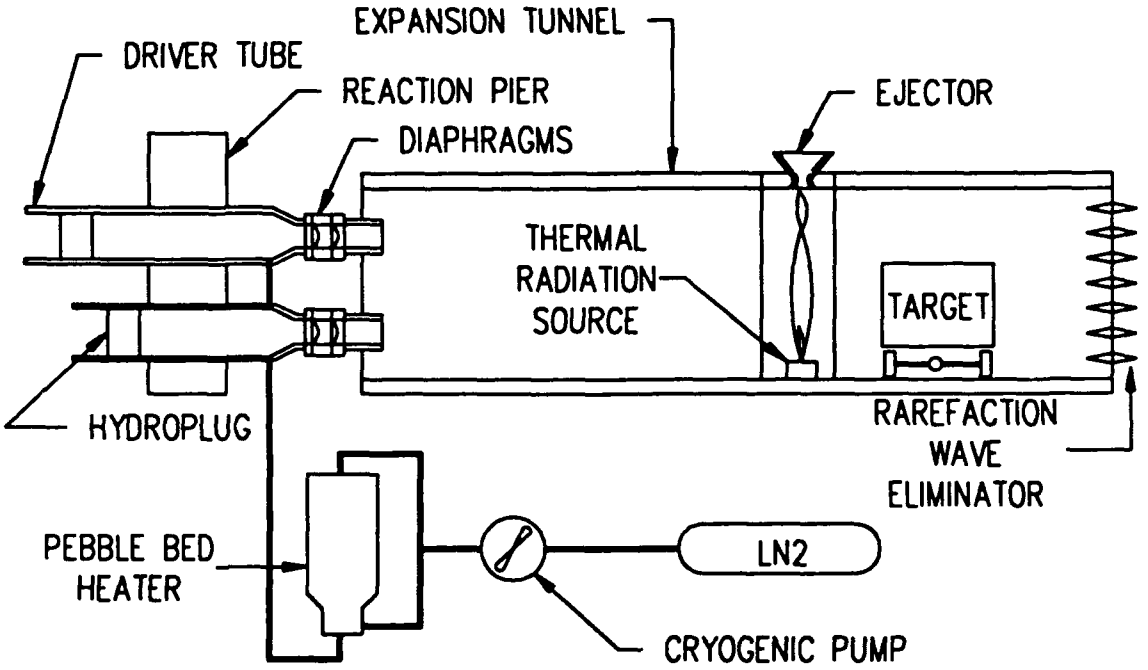

Figure 1. Schematic Diagram of the Large Blast/Thermal Simulator

II. The 1:57 Scale Large Blast Simulator

Part of BRL's research program has been to conduct experiments in small scale shock tubes in an effort to characterize the expected gas flow in the LB/TS. By performing experiments in a small scale simulator, a large number of inexpensive tests can be obtained in a relatively short period of time. Also, the use of a small simulator allows for easy modification and simple operation.

A 1:57 scale LBS (large blast simulator with no thermal radiation capability) has been used quite extensively at BRL to study the expected flow in the LB/TS and the effects that

design changes will have on the flow. Figure 2 is an illustration of the small scale blast simulator. Unlike the full scale LB/TS, the 1:57 scale LBS has a single driver and a circular expansion section. It models the nine driver LB/TS by lumping the available flow area at any given location into a single diameter.

The model was configured this way for the following reasons:

- An accurate three dimensional model would be difficult to construct and operate because multiple diaphragms and timing for diaphragm breaking would be difficult.
- A three dimensional experimental model would require three dimensional computer simulations which are complex and time consuming.
- Pipe sections for an axisymmetric model are readily available.
- An axisymmetric model can be simulated with one and two dimensional computer codes which require fewer computing resources.

With this two-dimensional axisymmetric model, the flow characteristics associated with the use of multiple drivers can not be studied. This disadvantage, however, was considered to be outweighed by the advantages of the simplified system described earlier.

A rarefaction wave eliminator was not used during the tests discussed in this report. Rather, a very long expansion section was employed. The use of a long expansion section does not eliminate the rarefaction wave. It simply delays the arrival of the rarefaction wave at the test section until after the period of interest has passed.

Driver gas heating was employed in the tests but the method by which the gas was heated differed from that intended for the LB/TS. Heating of the driver gas was accomplished by placing strip heaters on the outer surface of the driver tube. The desired driver gas temperature was obtained by turning the strip heaters on or off as required. One purpose of heating the driver gas is to provide density matching on either side of the contact surface between the gas originally in the driver and the shocked gas [4]. The other purpose of driver gas heating is to add energy to the driver gas which decreases the driver pressure required to produce a given shock overpressure. If the driver gas were not heated, a sudden increase would be seen in the dynamic pressure histories as the contact surface passed the measurement station. Since this phenomenon is not present in the dynamic pressure histories of a free-field, exponentially decaying blast wave, it is undesirable in the LB/TS. For this reason, an effort is made to provide contact surface density matching for all LBS experiments.

III. Experimental Measurements

An experimental parametric study was performed in the 1:57 scale LBS configured as shown in Figure 2. The purpose of this experimental study was to determine the performance of the 1:57 scale LBS in simulating free-field nuclear blast waves [5]. In this study,

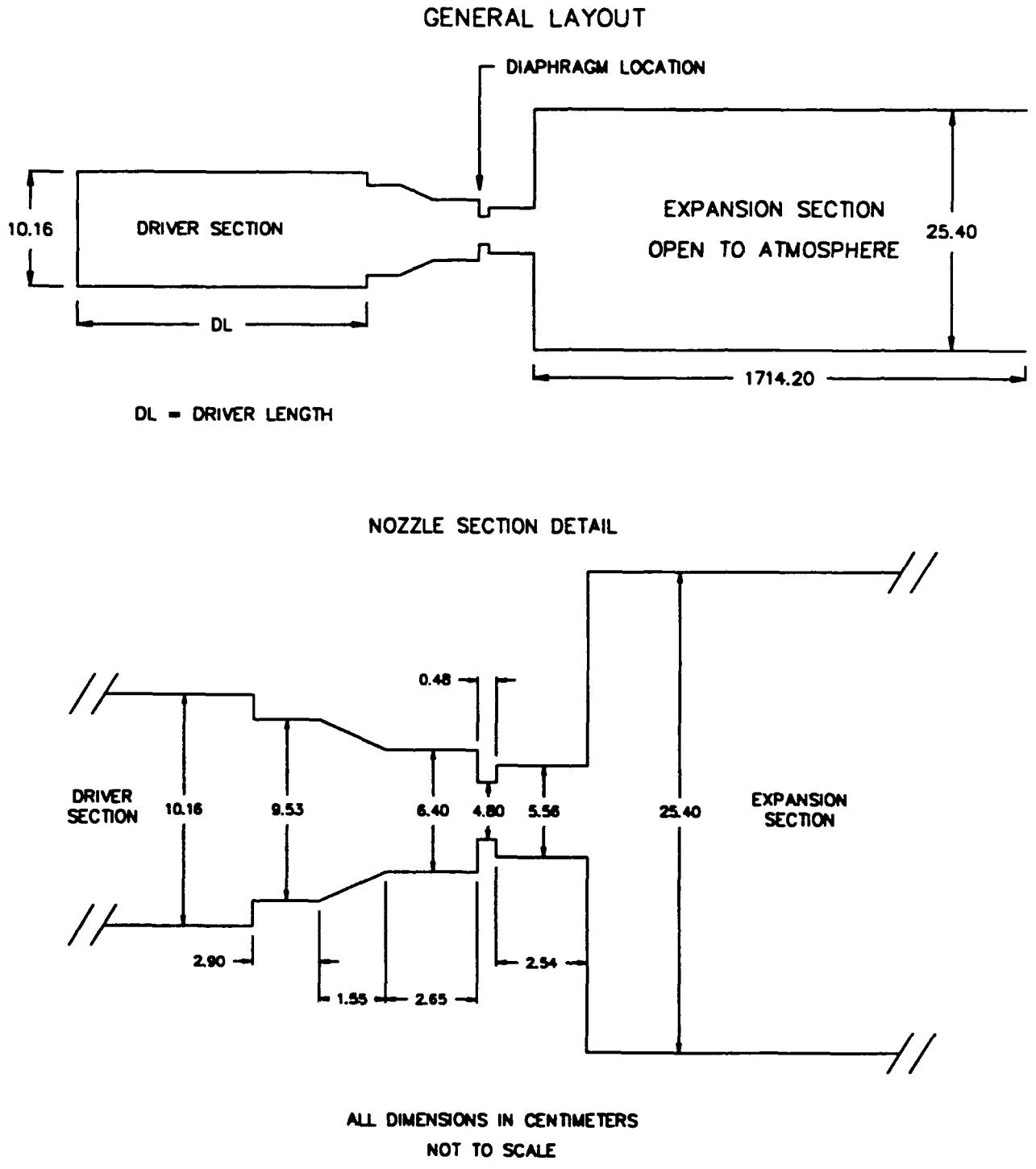

Figure 2. The 1:57 Scale Large Blast Simulator

the driver volume and initial driver pressure were varied with each test. In all the tests, attempts were made to set the driver temperature according to the contact surface density matching criterion discussed in Reference 4. Table 1 lists the initial test conditions for all the experiments included in the parametric study.

Table 1. Test Matrix

Shot Number	Driver Length (cm)	Ambient Pressure (kPa)	Ambient Temperature (K)	Driver Pressure (kPa)	Driver Temperature (K)
109	87.31	102.6	296.05	4378	399.15
110	87.31	102.3	298.05	6998	453.15
111	87.31	101.8	297.05	10170	493.15
112	87.31	102.0	297.15	12238	499.15
115	87.31	100.7	295.85	16030	535.15
116	66.83	102.3	294.85	4309	393.15
118	66.83	101.9	295.65	10617	498.15
119	66.83	101.8	295.95	13204	520.15
120	66.83	101.1	296.15	16651	568.15
126	33.97	102.2	297.55	4309	387.15
129	33.97	101.2	296.05	4412	385.15
127	33.97	101.2	298.05	6722	449.15
128	33.97	102.2	298.55	9308	487.15
130	33.97	101.4	297.85	11376	510.15
131	18.97	101.7	297.75	4344	388.15
132	18.97	101.5	297.75	6757	460.15
133	18.97	102.5	297.05	9997	495.15
134	18.97	103.1	298.75	11376	503.15
135	18.97	103.4	297.15	15686	502.15
136	6.03	102.6	297.05	4344	386.15
138	6.03	103.8	297.65	6895	434.15
137	6.03	102.8	297.75	9825	489.15
140	6.03	101.4	297.35	12928	497.15
139	6.03	103.3	294.05	15789	530.15

For all the experiments in the parametric study, pressure measurements were made at three different axial locations in the expansion section. Relative to the upstream end of the expansion section, the locations of these gages are 76.2 cm, 127.0 cm and 177.8 cm.

Two pressure gages were located at each of the three axial positions. A static pressure gage was located with its sensing element flush with the interior surface of the expansion section wall, 12.7 cm from the axis of symmetry. A stagnation probe was positioned at the half radius point, 6.35 cm from the axis of symmetry, and was facing upstream into the axial flow.

The location of the last pair of gages is important in that it is this location, when scaled, which corresponds to the location of the test station in the full scale LB/TS. The data recorded at this station was ultimately used to determine the shock overpressure and simulated yield for each test in the experimental parametric study. The data recorded at this station is the most significant in terms of LB/TS modelling. The data recorded at the remaining stations is also important in that it allows the analyst to see how the flow is changing as the shock wave travels down the expansion section.

By measuring the stagnation and static pressures at each axial location, the Mach number and dynamic pressure histories can be obtained. Accurate dynamic pressure histories are crucial to blast simulation because it is the dynamic pressure that causes targets to experience large displacements and overturning. In fact, the intended operating envelope of the LB/TS is based on dynamic pressure impulse for shock overpressures above 70 *kPa*. If the shock overpressure is below this value, the dynamic pressure history becomes difficult to measure experimentally.

In order to find the dynamic pressure one must first determine the Mach number, which can be calculated using the static and stagnation pressures. To obtain the Mach number history, one simply repeats the following set of calculations for each point in the pressure histories. Equation 1 assumes the flow is subsonic and that it is brought to rest at the probe's stagnation point through an isentropic process [6]. The isentropic relation expressed in Equation 1 can be solved for the square of the Mach number yielding Equation 2.

$$\frac{p_0}{p} = \left(1 + \frac{\gamma - 1}{2} M^2\right)^{\frac{\gamma}{\gamma - 1}} \tag{1}$$

$$M^2 = \left(\frac{2}{\gamma - 1}\right)\left[\left(\frac{p_0}{p}\right)^{(\gamma-1)/\gamma} - 1\right] \tag{2}$$

Where:

- M is the local Mach number of the gas,
- p_0 is the measured stagnation pressure,
- p is the measured static pressure, and
- γ is the ratio of specific heats (1.400).

If the local Mach number turns out to be greater than 1.0 from Equation 2, then the flow is considered to be supersonic, in which case Equation 3 should be used. Since Equation 3 has no closed form solution for M, a Newton iterative solver is used to determine its value for a given static and stagnation pressure.

$$\frac{p}{p_0} = \left(\frac{2\gamma}{\gamma + 1} M^2 - \frac{\gamma - 1}{\gamma + 1}\right)^{1/(\gamma-1)} \left(\frac{\gamma + 1}{2} M^2\right)^{(-\gamma)/(\gamma-1)} \tag{3}$$

Once the local Mach number is known, the dynamic pressure, q, can be calculated using Equation 4.

$$q = \frac{\gamma}{2} p M^2 \tag{4}$$

It was stated earlier that for low shock overpressures, the dynamic pressure becomes difficult to measure experimentally. As the shock overpressure is reduced, the difference between the stagnation pressure and the static pressure becomes small. Thus, the ratio of stagnation pressure to static pressure, p_0/p, approaches unity. As illustrated by Equation 2, the Mach number approaches zero as the pressure ratio, p_0/p, approaches unity. Since the dynamic pressure is a product of the Mach number and static pressure, as defined in Equation 4, its value will approach zero as well. This phenomenon is illustrated in Figure 3, which is a plot of stagnation pressure ratio, p_0/p_∞, and dynamic pressure ratio, q/p_∞, as a function of shock pressure ratio, p/p_∞, where p_∞ is equal to the ambient atmospheric pressure. As a result of this relationship between dynamic pressure and shock overpressure, small disturbances in the static and stagnation pressure histories caused by electronic noise or turbulence in the flow will be exaggerated in the experimental dynamic pressure history.

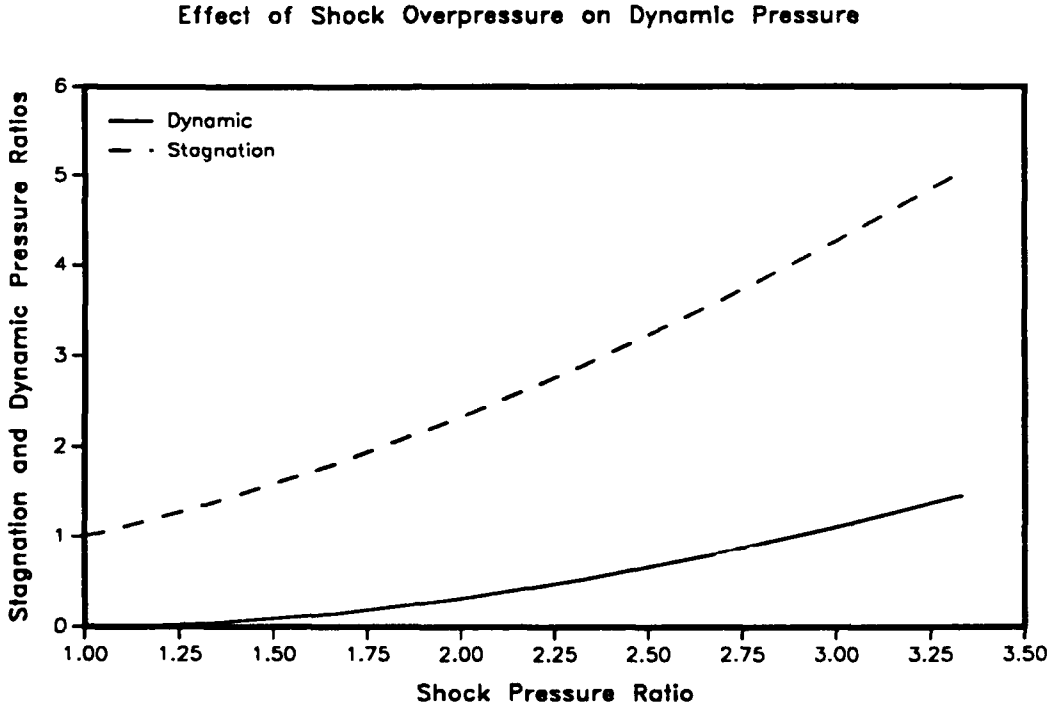

Figure 3. Effect of Shock Overpressure on Dynamic Pressure Ratio

IV. Calculations

To complement the experimental work, a computational parametric study was performed using the BRL-Q1D code [7]. The BRL-Q1D code was chosen for its relative ease of operation and quick execution time. A BRL-Q1D calculation was performed for each experiment in the program. This computational parametric study served two purposes. First, by comparing the experimental results to the calculated results, possible anomalies in the experimental records could be detected by examining those cases in which the experimental and calculational data suddenly diverged. Also, the experimental data could be used to validate the code so that further calculations could be performed. This validation would make it possible to study the flow characteristics of the 1:57 scale LBS for cases which are beyond the operating limits of the actual system.

For each of the experimental and computational results, the simulated weapon yield was calculated. This was done by multiplying the dynamic pressure impulse by the scaling factor of 57 and then applying the scaling laws presented by Glasstone and Dolan [8]. These scaling laws relate the blast parameters between different explosive yields. The resulting explosive yield is expressed in kilotons (kT). By comparing the experimental and computational results to a known standard (in this case 1 kT) of equal incident overpressure, the simulated yield for the test can be determined as illustrated in Equation 5.

$$\frac{I_1}{I_2} = \left(\frac{W_1}{W_2}\right)^{\frac{1}{3}} \tag{5}$$

In this equation, I_1 is the dynamic pressure impulse for the reference yield, W_1, and I_2 is the dynamic pressure impulse at the same pressure level for the predicted yield, W_2. Solving Equation 5 for W_2 yields Equation 6. Substitution of the reference yield W_1 equal to 1.0 kT leaves the predicted yield expressed in kilotons as a function of the measured impulse and the impulse of the reference yield.

$$W_2 = \left(\frac{I_2}{I_1}\right)^3 \tag{6}$$

One drawback of the BRL-Q1D code is that it is unable to accurately predict the peak shock overpressure of a given test. It has, however, demonstrated the ability to predict static overpressure impulse and dynamic pressure impulse with reasonable accuracy. The yield calculations discussed above are derived from the peak shock overpressure and the dynamic pressure impulse of a particular test. Since the overpressure results obtained from the BRL-Q1D code are known to be inaccurate, the simulated weapon yield for a BRL-Q1D calculation is computed from the experimentally measured peak shock overpressure and the BRL-Q1D dynamic pressure impulse.

V. Validation of the BRL-Q1D Code

For each experiment in the parametric study, a matching BRL-Q1D calculation was performed. A simulated explosive yield was calculated from the experimentally measured static overpressure and dynamic pressure impulse for the experiments and calculations. These results are summarized in Table 2. The second column in this table lists the full scale driver volume in cubic meters. This is the driver volume which would exist if the simulator shown in Figure 2 were enlarged by the scaling factor of 57. As in Table 1, the tests are listed in groups of equal driver volume with the largest equal to 1337 m^3 and the smallest of 117 m^3. The tests in each group are listed in order of increasing driver pressure.

Table 2. Experimental and Calculational Results

Shot Number	Full Scale Driver Volume (m^3)	Experimental Static Overpressure (kPa)	Scaled Experimental Dynamic Pressure Impulse ($kPa-s$)	Yield Based on Experiment Results (kT)	Scaled Q1D Dynamic Pressure Impulse ($kPa-s$)	Yield Based on Q1D Results (kT)
109	1337	109	20.634	1423.07	11.970	277.82
110	1337	150	37.107	2384.26	26.790	897.23
111	1337	180	67.830	7145.70	51.870	3195.42
112	1337	205	81.510	7669.99	N/A	N/A
115	1337	248	91.200	5320.72	N/A	N/A
116	1030	108	12.825	350.32	9.063	123.63
118	1030	173	33.060	959.44	42.522	2051.88
119	1030	215	54.720	1933.11	63.156	2972.09
120	1030	250	98.040	6474.45	N/A	N/A
126	536	104	N/A	N/A	4.560	18.54
129	536	107	5.244	24.47	4.805	18.83
127	536	138	9.519	54.48	9.576	55.46
128	536	156	14.364	119.11	16.587	183.41
130	536	178	22.800	282.38	23.598	313.08
131	311	103	3.340	7.51	2.622	3.63
132	311	138	6.498	17.40	5.301	9.45
133	311	166	9.804	29.77	10.260	34.12
134	311	183	11.400	32.88	12.215	40.45
135	311	223	18.639	69.18	22.059	114.67
136	117	89	1.254	0.73	0.798	0.19
138	117	110	2.451	2.37	1.653	0.73
137	117	134	2.850	1.68	2.907	1.79
140	117	152	4.845	4.95	4.845	4.95
139	117	198	5.586	2.83	6.544	4.55

The data in Table 2 is incomplete for tests 112, 115, 120 and 126. In tests 112, 115 and 120, the computational results could not be obtained because a recompression shock located upstream of the measurement station degraded the pressure histories at the measurement station. This made the recording of the dynamic pressure impulse for these calculations impossible. The effect of the recompression shock, however, was not observed in the experimental records for these tests. During test 126, the stagnation pressure gage failed to record the experimental data. This made the calculation of the dynamic pressure (and hence dynamic pressure impulse) impossible. The static pressure gage functioned properly in this test, allowing us to record the experimental shock overpressure which is listed in Table 2 as 104 *kPa*.

For each of the five driver volumes represented in Table 2, the results are illustrated in a chart of the scaled dynamic pressure impulse versus the static overpressure for the experimental and computational results. Figure 4 shows the results of the tests using a full scale driver volume equal to 1337 m^3. In this figure the dynamic pressure impulse curve for the calculational data follows that of the experimental data but at a lower value. As a result of these differences in impulse, the differences in the yield values are exaggerated as evidenced in Table 2. This exaggeration is caused by the nature of the scaling laws described earlier.

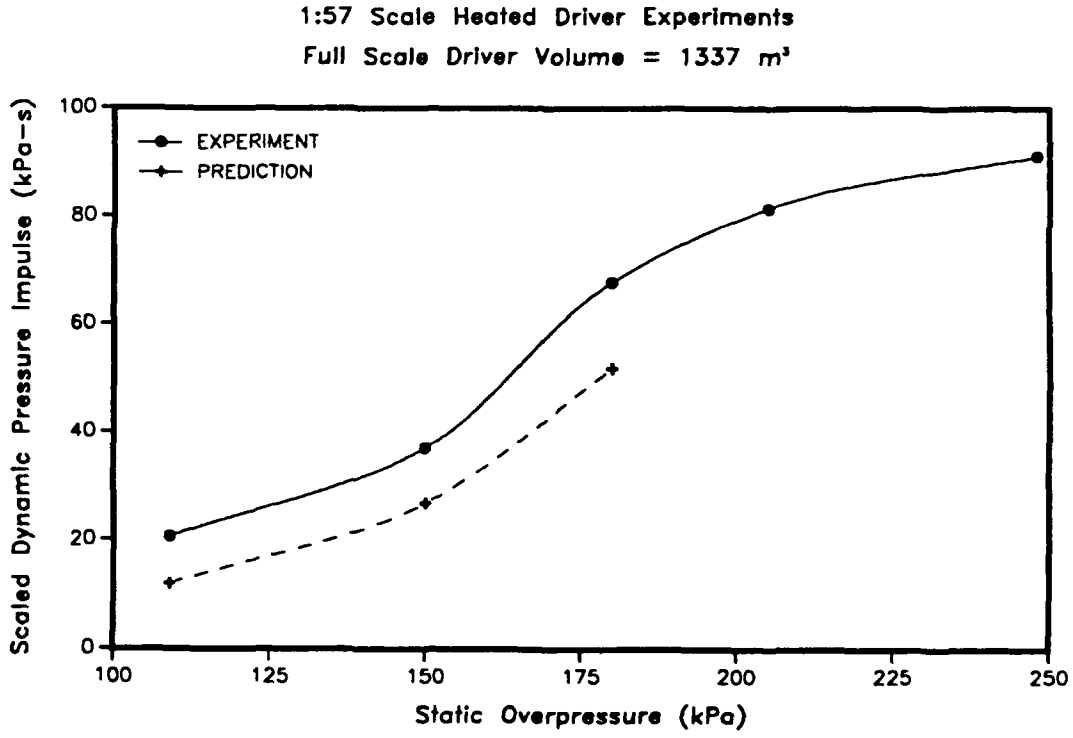

Figure 4. Dynamic Pressure Impulse for 1337 m^3 Driver Volume

As illustrated in Equation 6, the simulated yield is calculated from the cube of the ratio of the measured impulse and the reference impulse. Because of this cubing of the ratio, small variations in the measured impulse, I_2, may lead to large variations in the calculated

yield, W_2. In addition, as shock overpressure decreases, the dynamic pressure impulse for the reference yield decreases. As a result, the calculated yield is more sensitive to variations in impulse for small overpressures than for large overpressures. Thus, if the difference between the calculational and experimental impulse values is roughly constant, then the difference between the calculational and experimental yields will be largest at the lowest overpressures. For these reasons, when comparing computational data to experimental data, it is wise to directly compare the measured impulse rather than the calculated yield.

The results of the tests performed with an equivalent full scale driver volume of 1030 m^3 are shown in Figure 5. Once again, this figure compares the impulse results for the experiments and the calculations. As in the previous figure, the impulse results for the calculation seem to follow the trend set by the experiments. The differences between the experimental and computational impulse results fall between 15 and 29 percent.

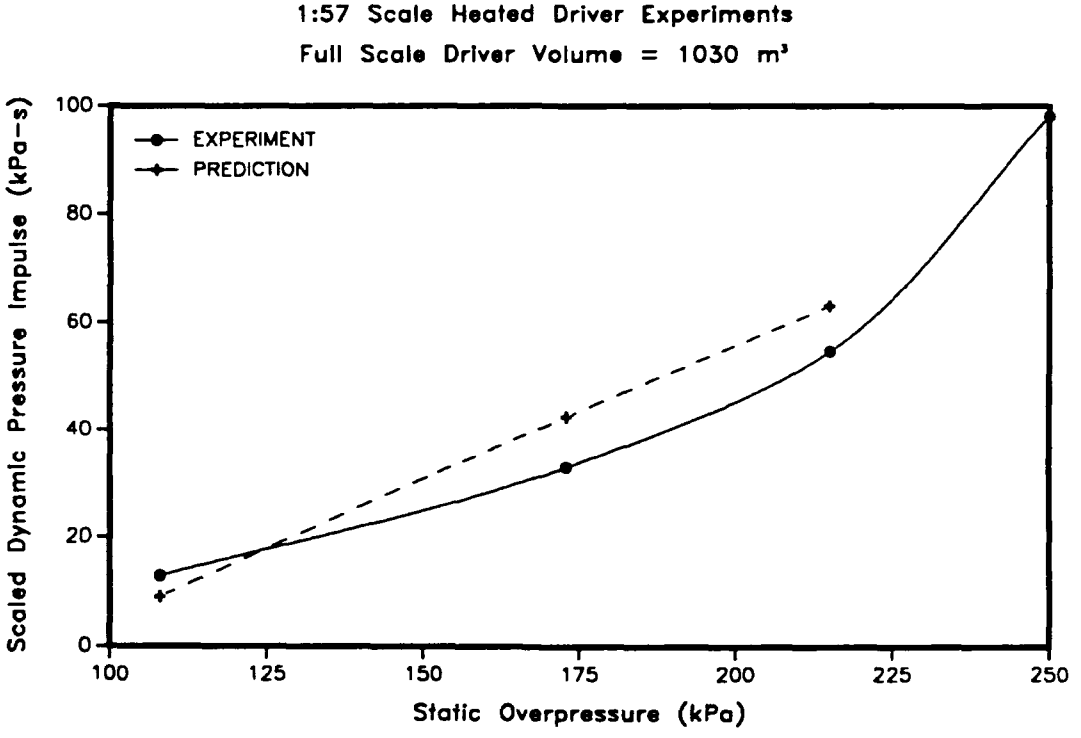

Figure 5. Dynamic Pressure Impulse for 1030 m^3 Driver Volume

The current design of the LB/TS employs a maximum driver volume of 584 m^3. The third set of tests in the parametric study was performed using an equivalent full scale driver volume of 536 m^3. The results from this set of tests should provide a good estimate of the expected performance of the full scale LB/TS. The results of these tests are shown in Figure 6. In this figure one can see that the dynamic pressure impulse measured in the experiments compares very well with the computational results. At 138 *kPa* this error is only 0.6 percent. The maximum impulse error in this set occurred at 156 *kPa* where it was 15.5 percent.

The final two sets of tests were performed using equivalent full scale driver volumes of

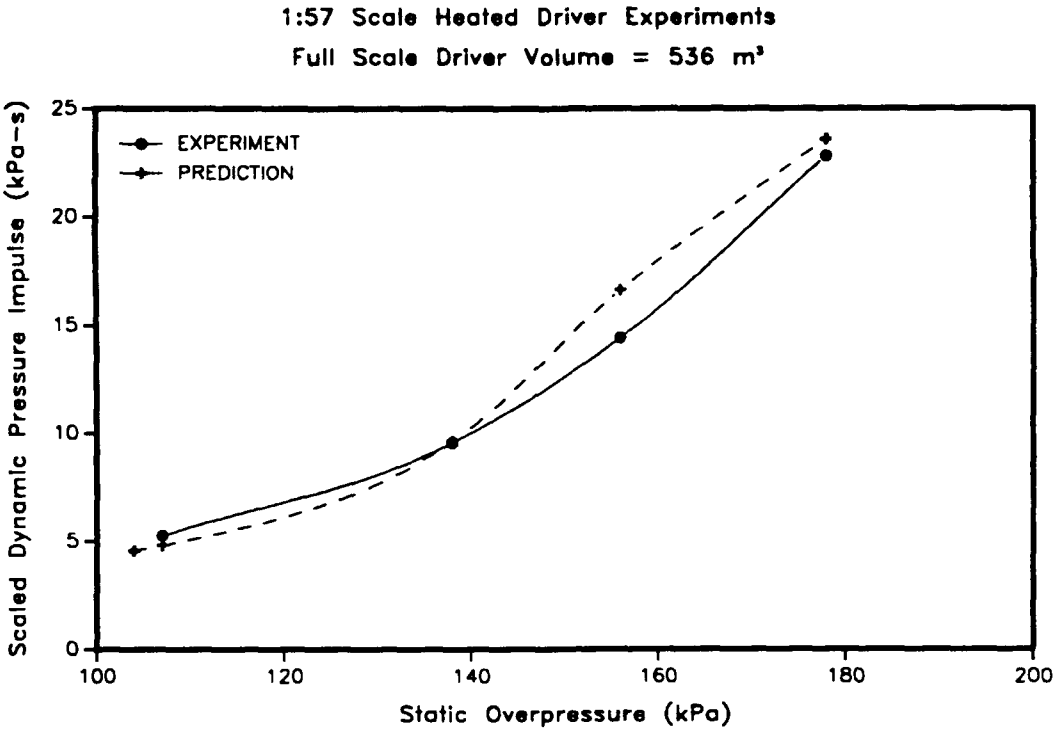

Figure 6. Dynamic Pressure Impulse for 536 m^3 Driver Volume

311 m^3 and 117 m^3. The results of these tests are summarized in Figures 7 and 8. For the 311 m^3 tests, the impulse error was a minimum of 4.6 percent at 103 *kPa* and a maximum of 21.5 percent at 166 *kPa*. The results for the 117 m^3 tests can be seen in Figure 8. In these tests, the experimental and computational data compare well at the higher overpressures where the minimum error is 0.0 percent and the maximum is 17.1 percent. At the two lowest overpressures, however, the impulse errors are greater than 30 percent.

VI. Driver Temperature Requirements

It was mentioned earlier that, in performing the experiments, an effort was made to conduct the tests in accordance with the contact surface density matching relationship described by Opalka in Reference 4. The ability of the experimentalist to meet this criterion will now be examined.

The density matching criterion is described in terms of driver pressure ratio and driver temperature ratio. The driver pressure ratio is defined as the sum of the driver overpressure plus the ambient pressure divided by the ambient pressure. The driver temperature ratio is defined as the absolute driver gas temperature divided by the absolute ambient temperature. The relationship between the driver pressure ratio and the driver temperature ratio for the test conditions is available in Table 3. In this table one can see that for many of the tests, the driver temperature ratio measured from the experiments was significantly less

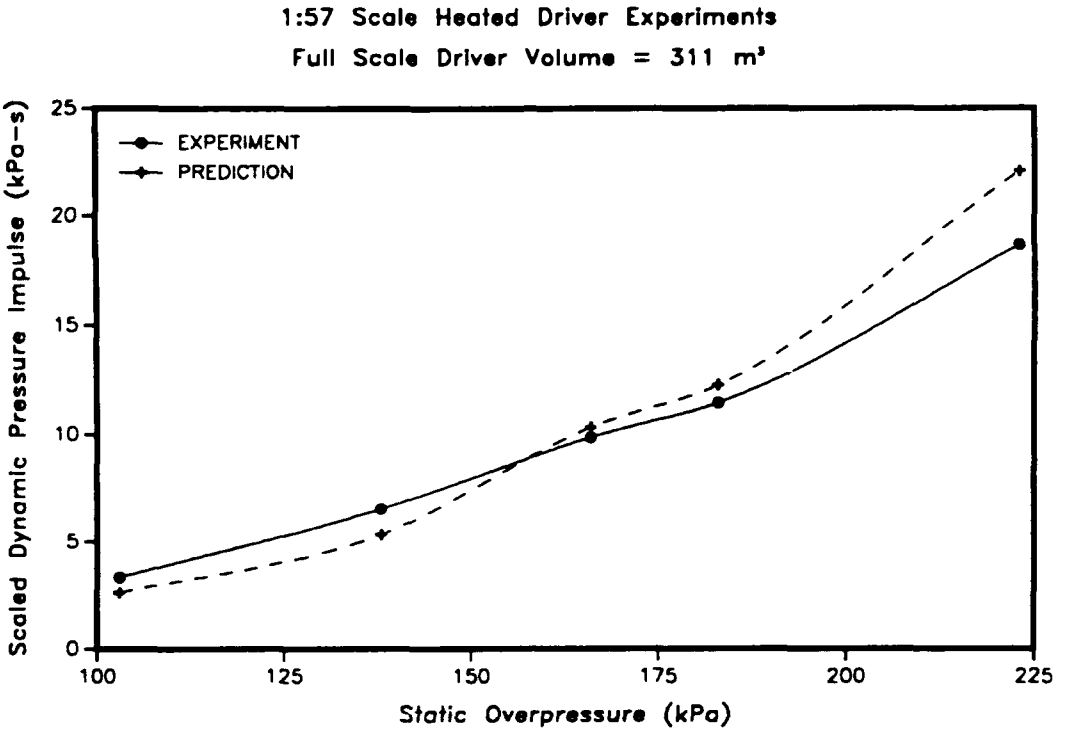

Figure 7. Dynamic Pressure Impulse for 311 m^3 Driver Volume

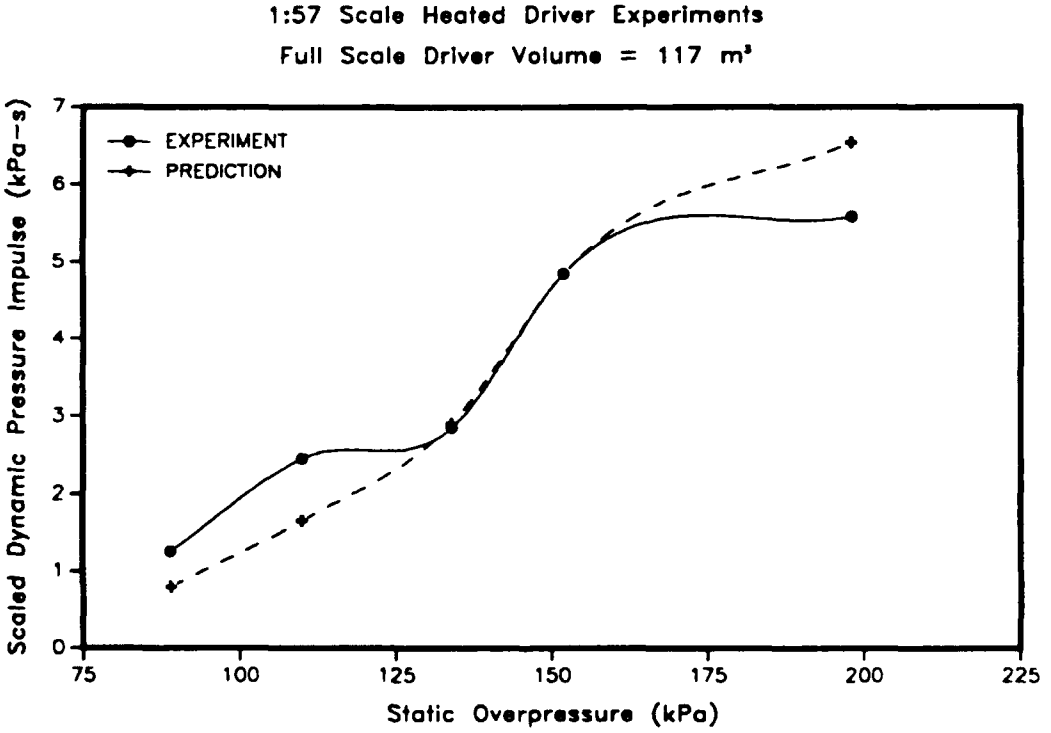

Figure 8. Dynamic Pressure Impulse for 117 m^3 Driver Volume

than the ideal temperature ratio as defined in Reference 4. This difference between the experimental and ideal temperature ratios is illustrated in Figure 9, which is a chart of the driver temperature ratio versus the driver pressure ratio for the experimental and ideal conditions. This figure illustrates that the difference between the experimental and ideal temperature ratio is greatest for the largest driver pressure ratios. From this chart, one can conclude that the heating apparatus used in the experiments was insufficient for heating the driver gas to the highest desired temperatures.

Table 3. Experimental and Ideal Driver Temperature Ratios

Shot Number	Driver Pressure Ratio	Experimental Driver Temperature Ratio	Ideal Driver Temperature Ratio
109	43.6716	1.3483	1.3036
110	69.4066	1.5204	1.6074
111	100.9018	1.6602	2.0107
112	120.9804	1.6798	2.1888
115	160.1857	1.8089	2.4475
116	43.1212	1.3334	1.2965
118	105.1904	1.6849	2.0565
119	130.7053	1.7576	2.2530
120	165.6983	1.9185	2.4839
126	43.1624	1.3011	1.2965
129	44.5968	1.3010	1.3109
127	67.4229	1.5070	1.5810
128	92.0763	1.6317	1.9038
130	113.1893	1.7128	2.1319
131	43.7139	1.3036	1.3036
132	67.5714	1.5454	1.5810
133	98.5317	1.6669	1.9822
134	111.3395	1.6842	2.1167
135	152.7021	1.6899	2.3981
136	43.3392	1.2999	1.3013
138	67.4258	1.4586	1.5810
137	96.5739	1.6428	1.9587
140	128.4951	1.6719	2.2384
139	153.8461	1.7999	2.4057

The primary purpose of heating the driver gas is to provide density matching on either side of the contact surface between the gas originally in the driver and the shocked gas. The secondary purpose is to decrease the driver pressure required to produce a given shock overpressure. If the driver gas is not sufficiently heated, a sudden increase will be present in the dynamic pressure histories. This effect can be seen in Figure 10 which is a dynamic

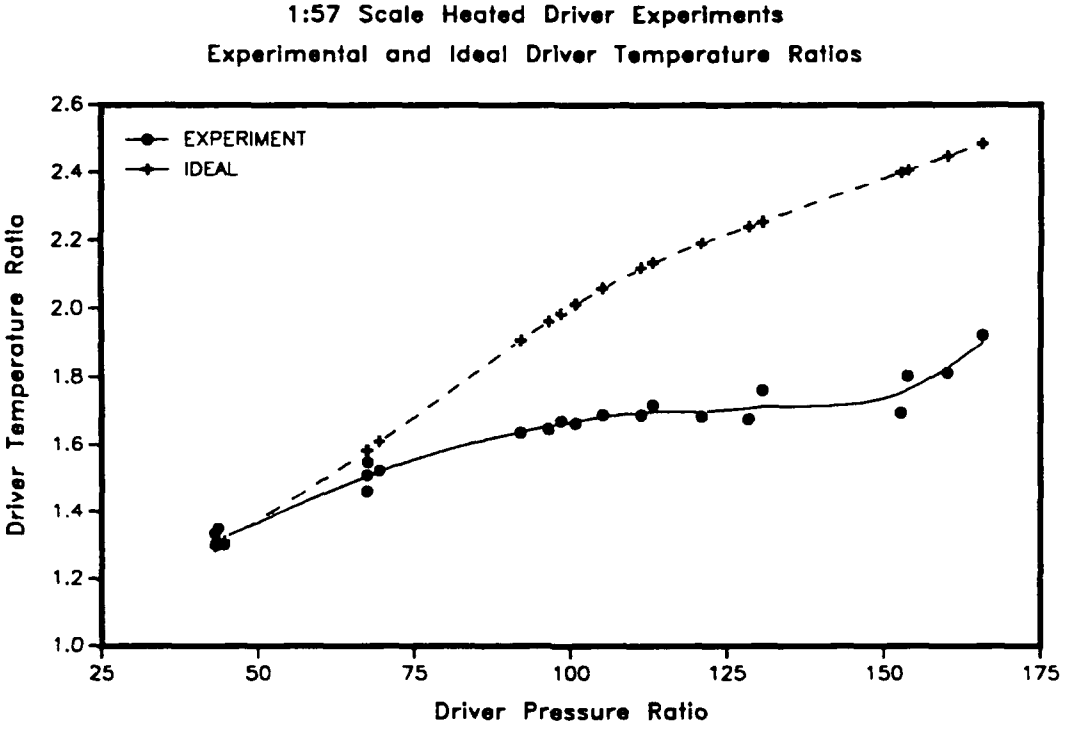

Figure 9. Experimental and Ideal Driver Temperature Ratios

pressure history from a BRL-Q1D calculation using the experimental driver temperature ratio. In this figure, the peak dynamic pressure is about 120 kPa and the dynamic pressure impulse is about 0.70 $kPa - s$. The sudden increase in dynamic pressure is labeled as a "Cold Gas Effect" in the figure. This effect is caused by the passing of the contact surface through the measurement station. This cold gas effect creates a net increase in dynamic pressure impulse.

Another dynamic pressure history is shown in Figure 11. This history is the result of a subsequent BRL-Q1D calculation which employed the ideal driver temperature ratio. As a direct result of the additional driver gas heating, the peak dynamic pressure has increased to about 140 kPa and the cold gas effect is gone. The dynamic pressure impulse for this calculation is about 0.66 $kPa - s$ which is less than that of the calculation using the experimental temperature ratio.

Since the additional heating caused the incident shock overpressure to increase and the dynamic pressure impulse to decrease, the simulated yield for the calculation using the ideal temperature ratio will be less than that which used the experimental temperature ratio. For this reason, performance predictions for the full scale LB/TS which are derived from the experimental results discussed earlier may not be accurate for the higher shock overpressures.

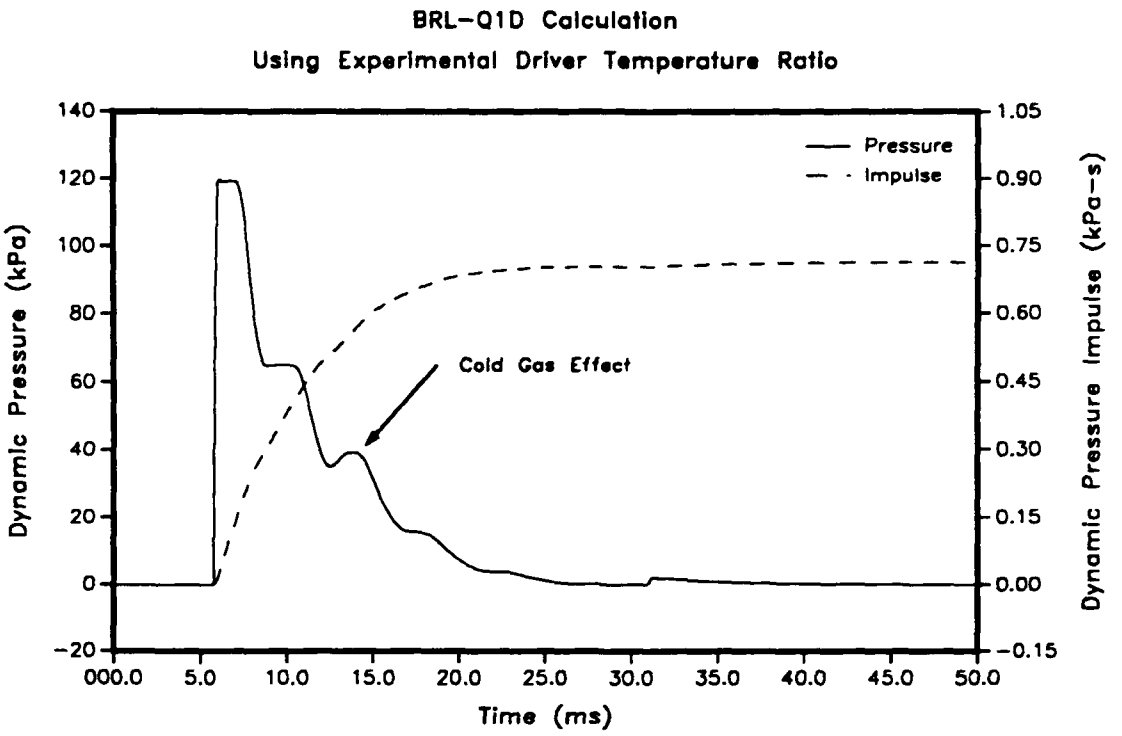

Figure 10. Dynamic Pressure Using Experimental Temperature Ratio

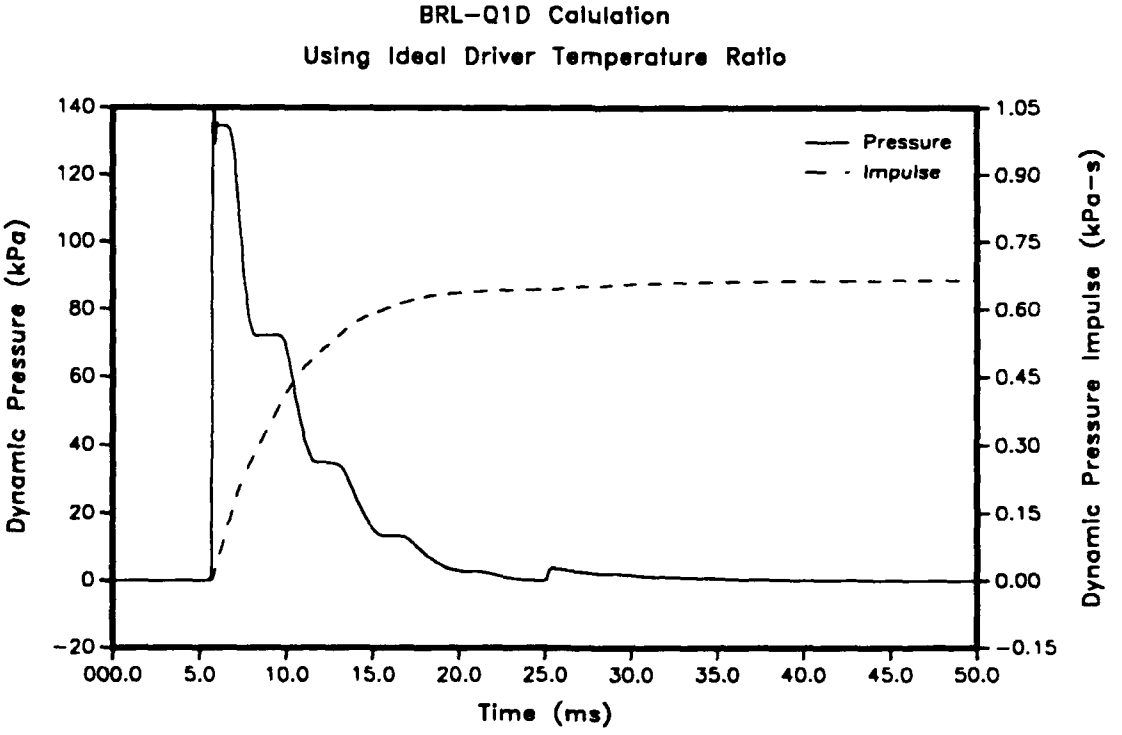

Figure 11. Dynamic Pressure Using Ideal Temperature Ratio

VII. Calculations Using Ideal Driver Temperatures

In an effort to develop a better estimate of the expected performance of the LB/TS, a second computational parametric study was performed with the BRL-Q1D code. This parametric study employed the ideal driver temperature ratio for each test rather than the experimental driver temperature ratio. No additional calculations were performed for the low overpressure cases in which the experimental and ideal driver temperature ratios were very close.

The results of this second computational parametric study are summarized in Table 4. In this table, the tests for which a second calculation was performed are noted with an asterisk (*) next to the shot number. As in Table 2, the computational data for test 115 was not obtained because of the presence of a recompression shock which destroyed the pressure histories at the measurement station. However, the data for tests 112 and 120 were obtained in the second computation study, whereas they were lost in the first study due to the effect of a recompression shock. Apparently the additional driver gas heating used in the second calculation helped to suppress the effect of this recompression shock at the measurement station. This phenomenon is documented in Reference 1.

Two figures are given for each set of tests corresponding to a given driver volume. The first of each pair of figures is a plot of the scaled dynamic pressure impulse versus the static overpressure. The second figure in each pair is a chart of the simulated weapon yield versus the static overpressure. These charts are presented in Figures 12 through 21.

Using the ideal driver temperature ratio in these calculations eliminated the cold gas effect discussed earlier. As a result, the dynamic pressure impulse for these calculations is lower than that obtained from the previous set of calculations. This reduction in dynamic pressure impulse is evident in the charts which plot the impulse against shock overpressure (Figures 12, 14, 16, 18 and 20). It is interesting to note that the relationship between dynamic pressure impulse and shock overpressure is almost linear for all five sets of tests.

It was previously stated that heating the driver gas to the ideal temperature ratio would cause the initial yield estimates to decrease. As illustrated in Figures 13, 15, 17, 19 and 21 the predictions of simulated weapon yield from the second study are significantly less than those of the earlier study. For example, the yield for test 119 drops from 2972 kT in the earlier study to 1288 kT in the second study. This reduction in yield is evident in other tests as well. It is also interesting to note that in all the yield versus shock overpressure figures, the curves are approximately asymptotic in nature (their slopes decrease with increasing shock overpressure).

Table 4. Results of Q1D Calculations Using Ideal Driver Temperature

Shot Number	Full Scale Driver Volume (m^3)	Expected Static Overpressure (kPa)	Scaled Q1D Dynamic Pressure Impulse ($kPa - s$)	Yield Based on Q1D Results (kT)
109	1337	109	11.970	277.82
110	1337	150	26.790	897.82
111*	1337	191	46.102	1801.50
112*	1337	227	60.990	2243.21
115*	1337	N/A	N/A	N/A
116	1030	108	9.063	123.63
118*	1030	184	38.190	1161.93
119*	1030	235	53.010	1288.04
120*	1030	275	75.240	2094.39
126	536	104	4.560	18.54
129	536	107	4.805	18.83
127	536	138	9.576	55.46
128*	536	163	16.530	154.48
130*	536	192	22.230	195.41
131	311	103	2.620	3.63
132	311	138	5.301	9.45
133*	311	173	9.975	27.12
134*	311	183	12.141	39.72
135*	311	241	19.380	59.16
136	117	89	0.798	0.19
138*	117	110	1.653	0.73
137*	117	137	2.850	1.55
140*	117	159	4.560	3.48
139*	117	198	5.985	3.48
* Calculations performed in second Q1D study.				

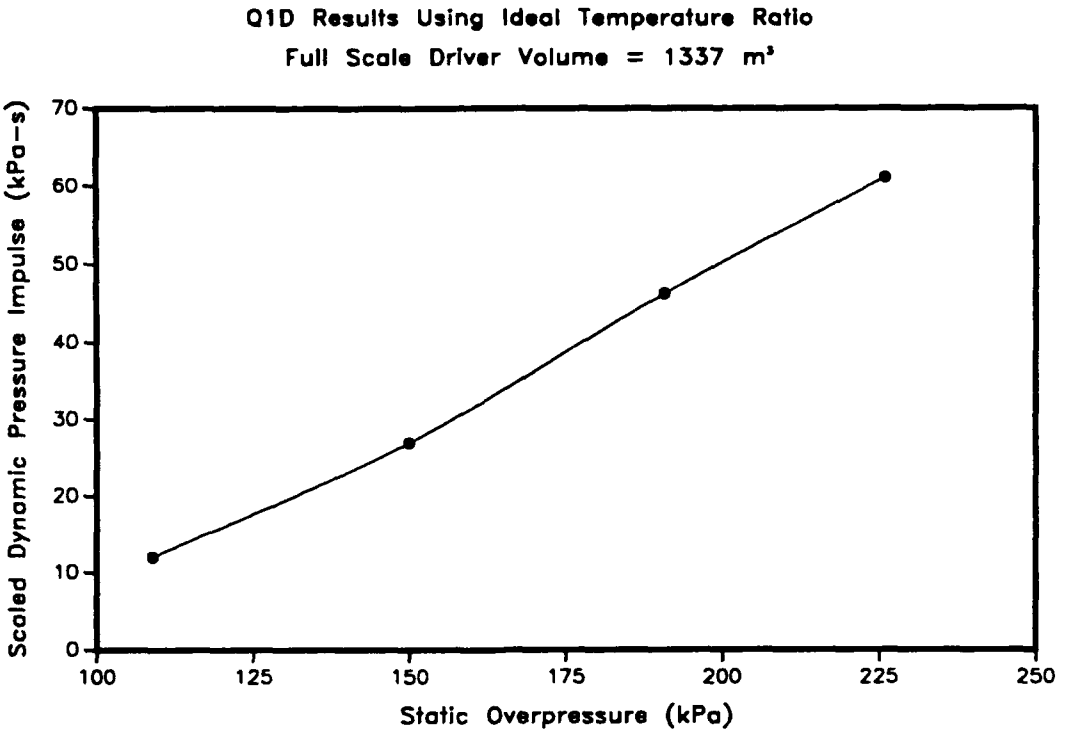

Figure 12. Impulse for 1337 m^3 Driver Using Ideal Temperature Ratio

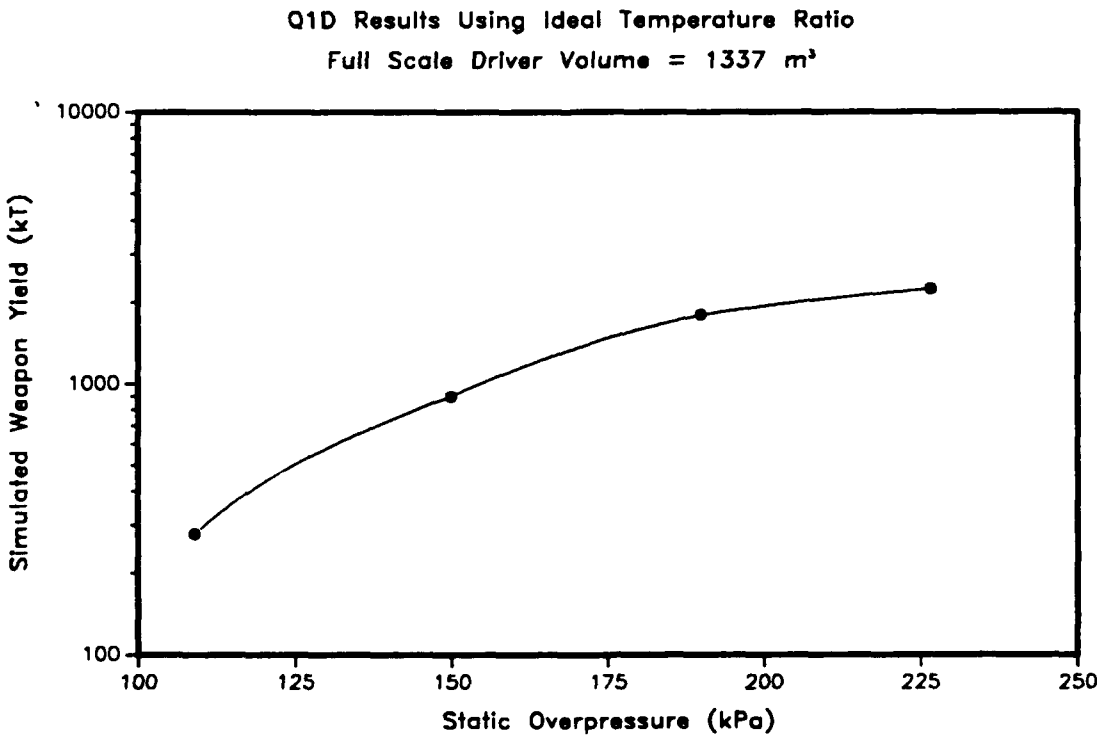

Figure 13. Yield for 1337 m^3 Driver Using Ideal Temperature Ratio

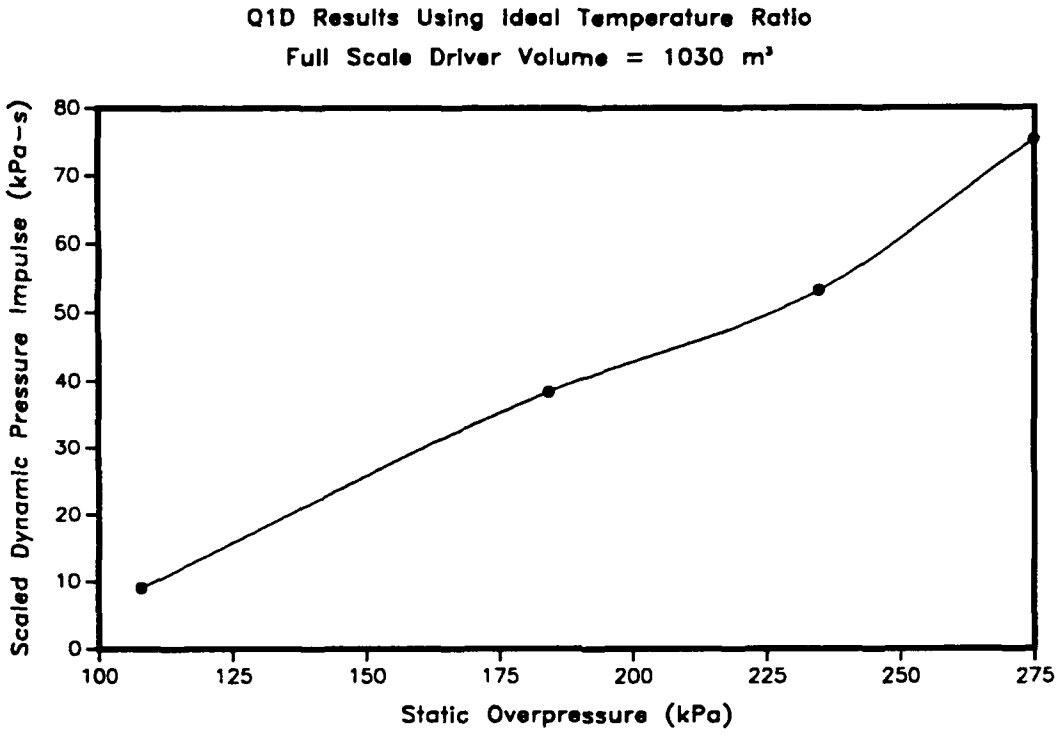

Figure 14. Impulse for 1030 m^3 Driver Using Ideal Temperature Ratio

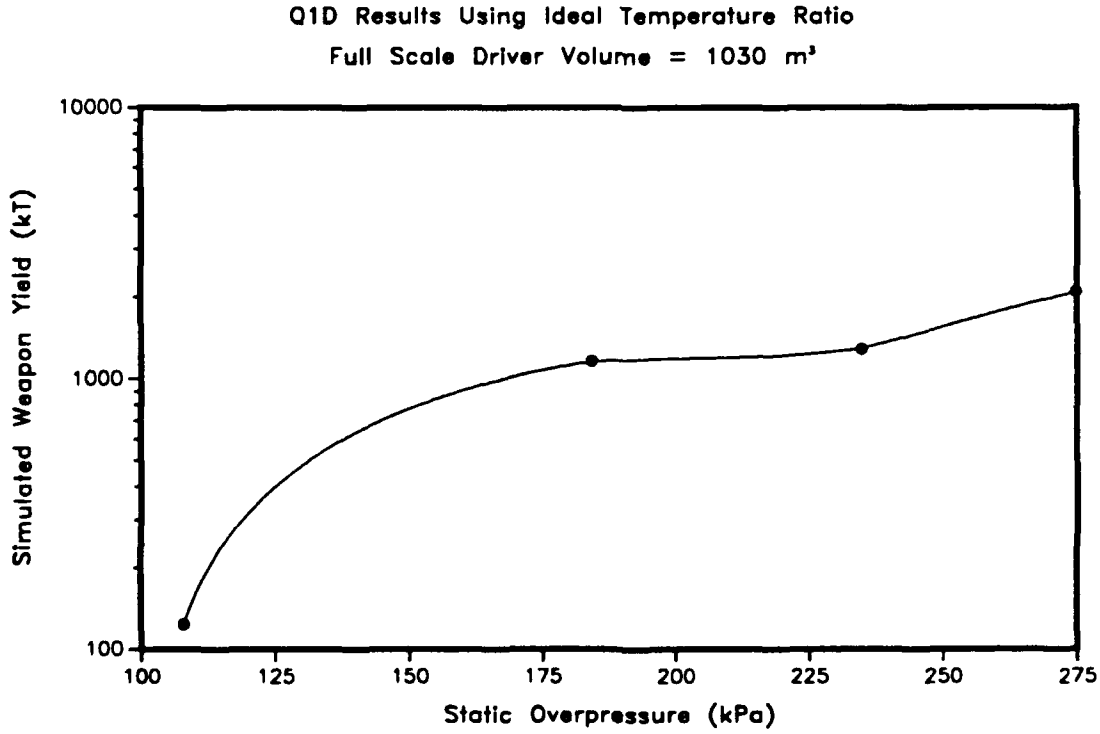

Figure 15. Yield for 1030 m^3 Driver Using Ideal Temperature Ratio

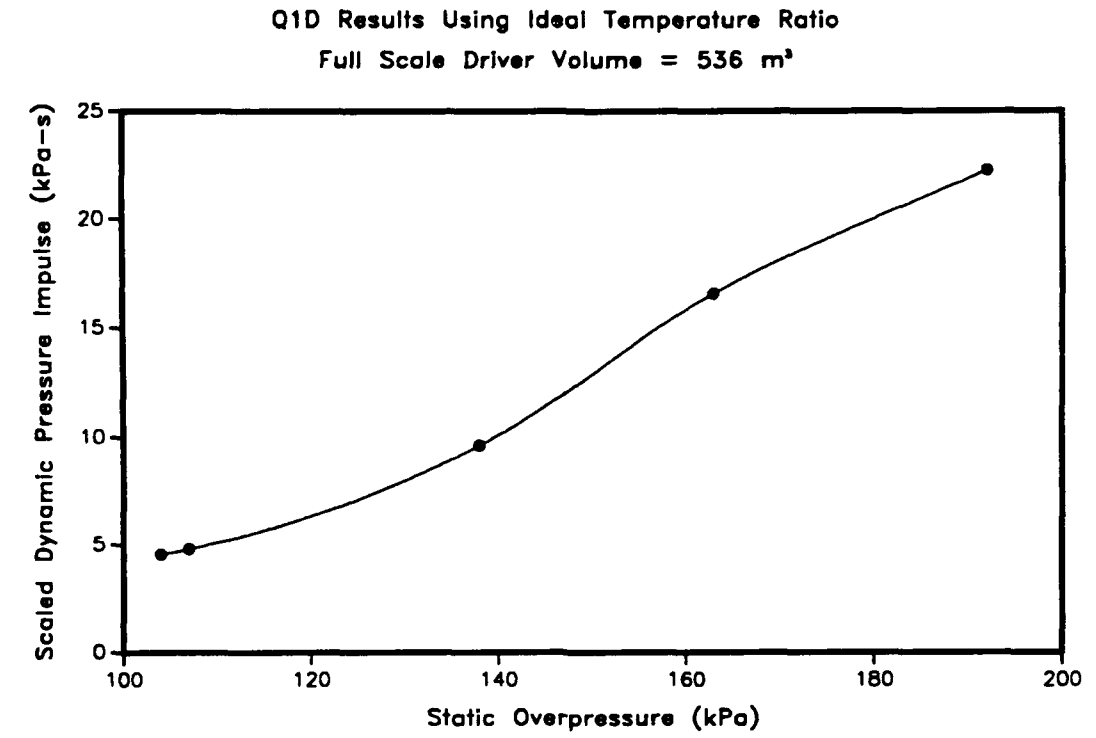

Figure 16. Impulse for 536 m^3 Driver Using Ideal Temperature Ratio

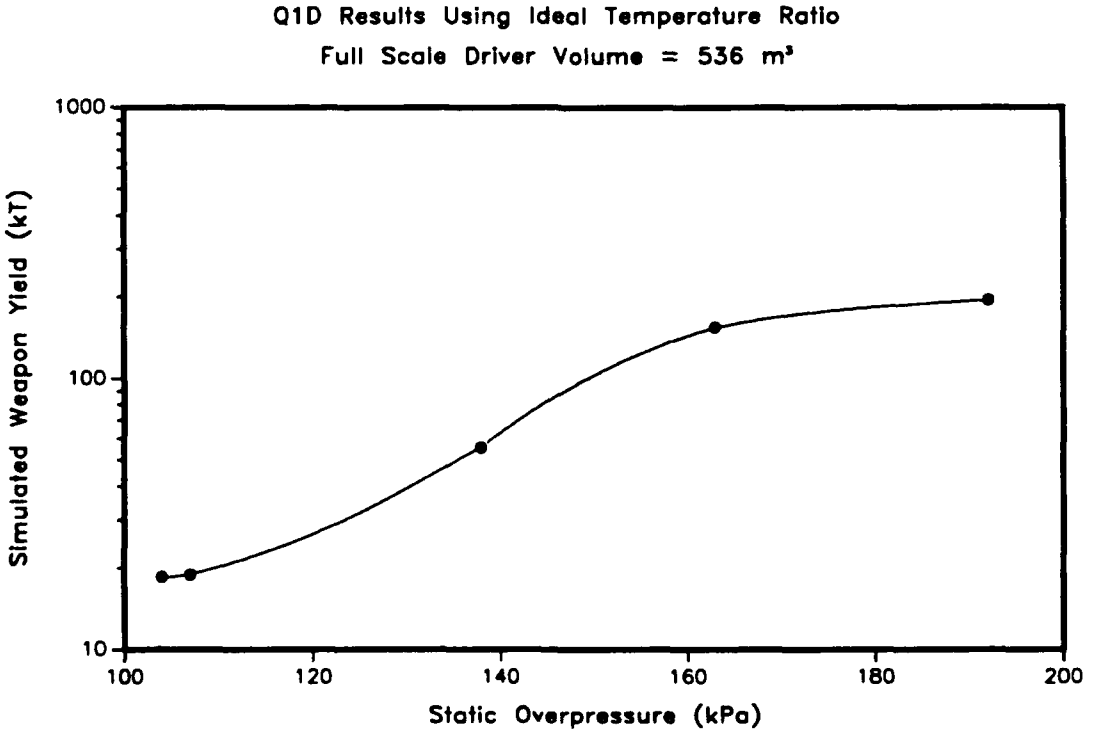

Figure 17. Yield for 536 m^3 Driver Using Ideal Temperature Ratio

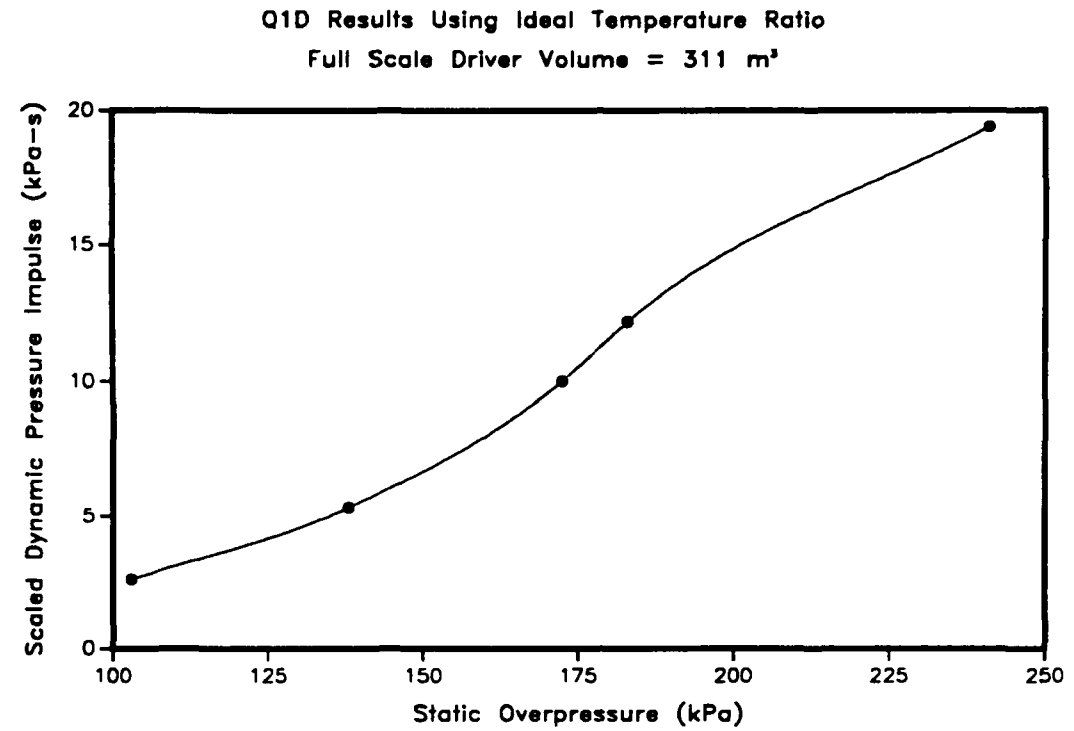

Figure 18. Impulse for 311 m^3 Driver Using Ideal Temperature Ratio

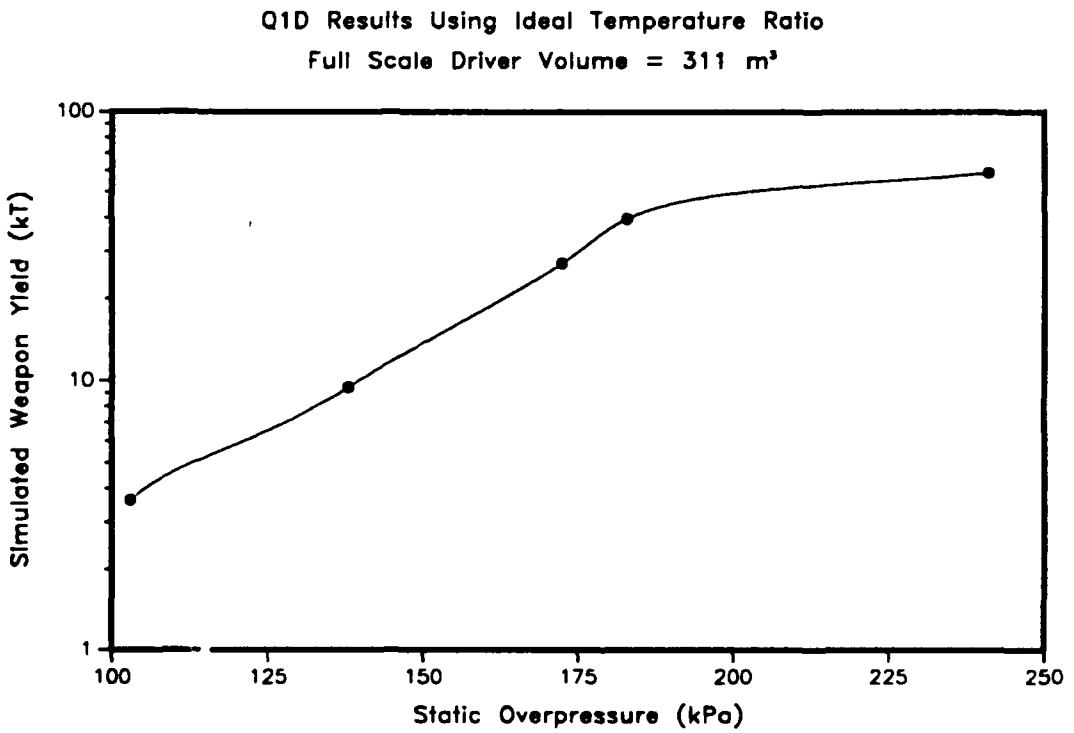

Figure 19. Yield for 311 m^3 Driver Using Ideal Temperature Ratio

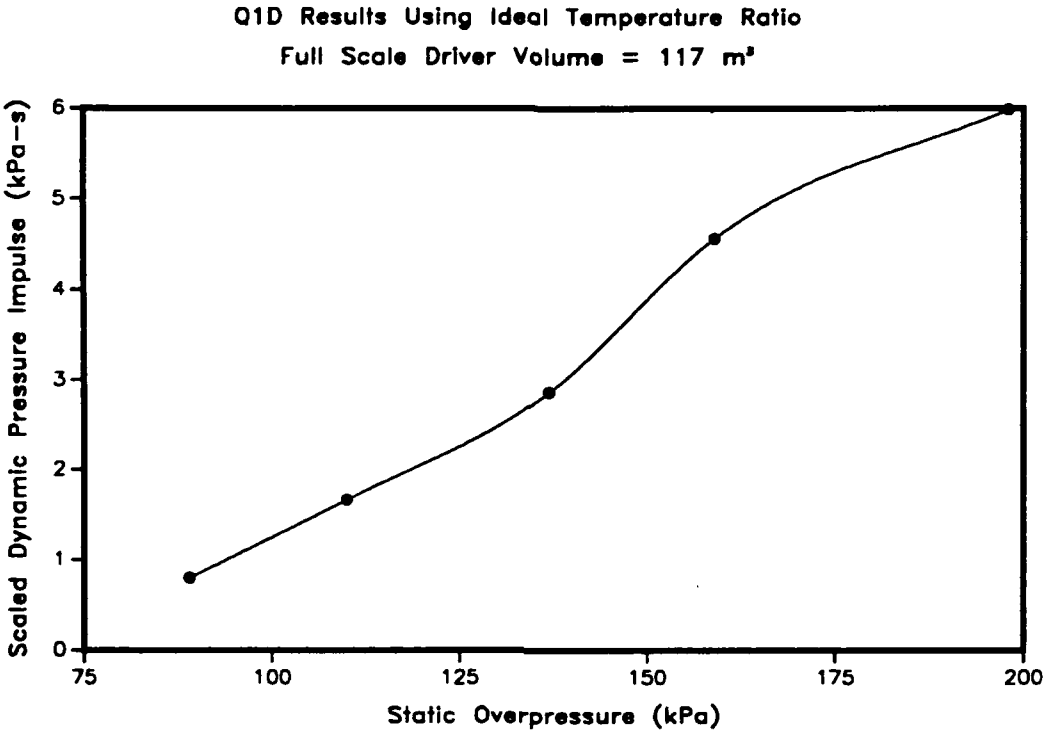

Figure 20. Impulse for 117 m^3 Driver Using Ideal Temperature Ratio

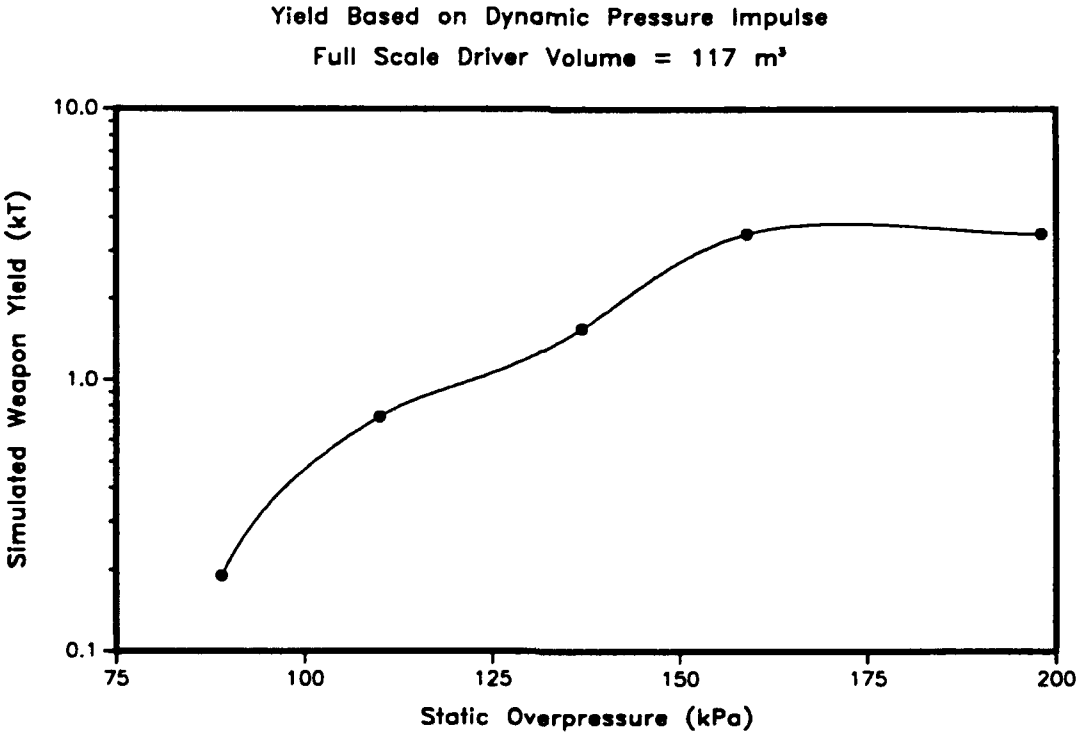

Figure 21. Yield for 117 m^3 Driver Using Ideal Temperature Ratio

VIII. Conclusion

This report has attempted to analyze the results of two calculational studies performed using the BRL-Q1D code. The first study attempted to match the results obtained from an experimental parametric study. The purpose of this experimental study was to validate the ability of the BRL-Q1D code to predict the static and dynamic pressure impulse in the 1:57 scale Large Blast Simulator. The results of the first computational parametric study were analyzed and found to be in reasonable agreement with the experimental results.

During the experimentation, attempts were made to heat the driver gas according to a predetermined relationship between driver gas pressure and driver gas temperature. When comparing the experimental conditions to the ideal pressure/temperature relationship, the driver gas was found to have been insufficiently heated for many of the high pressure tests. Failure to fully heat the driver gas can artificially increase the measured dynamic pressure impulse. This effect is subtle and can go unnoticed in experimentally measured dynamic pressure records.

The nature of the scaling laws which are used to calculate the simulated weapon yield indicates that tests with insufficient driver gas heating may produce overly optimistic estimates for the performance of the LB/TS. In an attempt to improve the performance estimates, a second computational parametric study was performed. This study employed the ideal driver gas pressure/temperature relationship in the initial conditions. The results of this study prove that the initial performance estimates were indeed optimistic due to the insufficient driver gas heating. The revised performance predictions which resulted from this second study were significantly lower than those from the experiments and the initial computational parametric study.

References

1. Pearson, R.J., Opalka, K.O. and Hisley, D.M., "Design Studies of Drivers for the U.S. Large Blast/Thermal Simulator," Proceedings of the 9^{th} International Symposium on the Military Applications of Blast Simulation, 23-27 September 1985, Atomic Weapons Research Establishment Foulness, Southend-on-Sea, Essex, England SS3 9XE.

2. Osofsky, I.B., Mason, G.P., Tanaka, M.J. and Hove, D.T., "Development of a Pebble-Bed Liquid Nitrogen Evaporator/Superheater for the Scaled Large Blast/Thermal Simulator (LB/TS) Facility," BRL-CR (in reproduction), US Army Ballistic Research Laboratory, Aberdeen Proving Ground, Maryland 21005.

3. Schraml, S.J. and Pearson, R.J., "Small Scale Shock Tube Experiments Using a Computer Controlled Active Rarefaction Wave Eliminator," BRL-TR-3149, US Army Ballistic Research Laboratory, Aberdeen Proving Ground, Maryland 21005, September 1990.

4. Opalka, K.O., "Large Blast and Thermal Simulator Advanced Concept Driver Design by Computational Fluid Dynamics," BRL-TR-3026, US Army Ballistic Research Laboratory, Aberdeen Proving Ground, Maryland 21005, August 1989.

5. Coulter, G.A. and Pearson, R.J., "Blast Parametric Study Using a 1:57 Scale Single Driver Model of a Large Blast Simulator - Part II," BRL-TR (to be published), US Army Ballistic Research Laboratory, Aberdeen Proving Ground, Maryland 21005.

6. Liepmann H.W. and Roshko A., 1957, "Elements of Gas Dynamics," John Wiley & Sons, Inc., page 148.

7. Opalka, K.O. and Mark, A., "The BRL-Q1D Code: A Tool for the Numerical Simulation of Flows in Shock Tubes with Variable Cross-Sectional Areas," BRL-TR-2763, US Army Ballistic Research Laboratory, Aberdeen Proving Ground, Maryland 21005, October 1986.

8. Glasstone, S. and Dolan, P.J. - Editors, "The Effects of Nuclear Weapons," Department of Army Pamphlet No. 50-3, HQ, Department of Army, March 1977.

INTENTIONALLY LEFT BLANK.

No of Copies	Organization
2	Administrator Defense Technical Info Center ATTN: DTIC-DDA Cameron Station Alexandria, VA 22304-6145
1	HQDA (SARD-TR) WASH DC 20310-0001
1	Commander U.S. Army Materiel Command ATTN: AMCDRA-ST 5001 Eisenhower Avenue Alexandria, VA 22333-0001
1	Commander U.S. Army Laboratory Command ATTN: AMSLC-DL 2800 Powder Mill Road Adelphi, MD 20783-1145
2	Commander U.S. Army Armament Research, Development, and Engineering Center ATTN: SMCAR-IMI-I Picatinny Arsenal, NJ 07806-5000
2	Commander U.S. Army Armament Research, Development, and Engineering Center ATTN: SMCAR-TDC Picatinny Arsenal, NJ 07806-5000
1	Director Benet Weapons Laboratory U.S. Army Armament Research, Development, and Engineering Center ATTN: SMCAR-CCB-TL Watervliet, NY 12189-4050
(Unclass. only) 1	Commander U.S. Army Armament, Munitions and Chemical Command ATTN: AMSMC-IMF-L Rock Island, IL 61299-5000
1	Director U.S. Army Aviation Research and Technology Activity ATTN: SAVRT-R (Library) M/S 219-3 Ames Research Center Moffett Field, CA 94035-1000

No of Copies	Organization
1	Commander U.S. Army Missile Command ATTN: AMSMI-RD-CS-R (DOC) Redstone Arsenal, AL 35898-5010
1	Commander U.S. Army Tank-Automotive Command ATTN: ASQNC-TAC-DIT (Technical Information Center) Warren, MI 48397-5000
1	Director U.S. Army TRADOC Analysis Command ATTN: ATRC-WSR White Sands Missile Range, NM 88002-5502
(Class. only)] 1	Commandant U.S. Army Infantry School ATTN: ATSH-CD (Security Mgr.) Fort Benning, GA 31905-5660
(Unclass. only)] 1	Commandant U.S. Army Infantry School ATTN: ATSH-CD-CSO-OR Fort Benning, GA 31905-5660
1	Air Force Armament Laboratory ATTN: AFATL/DLODL Eglin AFB, FL 32542-5000
	Aberdeen Proving Ground
2	Dir, USAMSAA ATTN: AMXSY-D AMXSY-MP, H. Cohen
1	Cdr, USATECOM ATTN: AMSTE-TD
3	Cdr, CRDEC, AMCCOM ATTN: SMCCR-RSP-A SMCCR-MU SMCCR-MSI
1	Dir, VLAMO ATTN: AMSLC-VL-D
10	Dir, BRL ATTN: SLCBR-DD-T

No of Copies	Organization
1	Director of Defense Research & Engineering ATTN: DD/TWP Washington, DC 20301
1	Assistant Secretary of Defense (Atomic Energy) ATTN: Document Control Washington, DC 20301
1	Chairman Joint Chiefs of Staff ATTN: J-5, R&D Div Washington, DC 20301
2	Deputy Chief of Staff for Operations and Plans ATTN: Technical Library Director of Chemical and Nuclear Operations Department of the Army Washington, DC 20310
1	Director Defense Advanced Research Projects Agency ATTN: Tech Lib 1400 Wilson Boulevard Arlington, VA 22209
2	Director Federal Emergency Management Agency ATTN: Public Relations Office Technical Library Washington, DC 20472
1	Director Defense Intelligence Agency ATTN: DT-2/Wpns & Sys Div Washington, DC 20301
1	Director National Security Agency ATTN: R15, E. F. Butala Ft. George G. Meade, MD 20755
9	Director Defense Nuclear Agency ATTN: CSTI, Tech Lib DDIR DFSP, Ullrich NANS OPNA SPSD, Goering Rohr SPTD, Kennedy Hrinishin Washington, DC 20305
3	Commander Field Command, DNA ATTN: FCPR FCTMOF NMHE/CDR Lund Kirtland AFB, NM 87115
10	Central Intelligence Agency DIR/DB/Standard ATTN: GE-47 HQ Washington, DC 20505
1	Commandant Interservice Nuclear Weapons School ATTN: Technical Library Kirtland AFB, NM 87115

No of Copies	Organization
4	Director US Army Harry Diamond Labs ATTN: SLCHD-NW-RA, L. Belliveau SLCHD-NW-P, Corrigan Gwaltney SLCHD-TA-L, Tech Lib 2800 Powder Mill Road Adelphi, MD 20783-1197
1	Director US Army Laboratory Command USASMO ATTN: SLCSM-SE, J. Orsega 2800 Powder Mill Road Adelphi, MD 20783-1197
2	Commander, USACECOM ATTN: AMSEL-RD AMSEL-RO-TPPO-P Fort Monmouth, NJ 07703-5301
1	Commander, USACECOM R&D Technical Library ATTN: ASQNC-ELC-I-T, Myer Center Fort Monmouth, NJ 07703-5301
1	Director US Army Missile and Space Intelligence Center ATTN: AIAMS-YDL Redstone Arsenal, AL 35898-5500
1	Commander US Army Foreign Science and Technology Center ATTN: Research & Data Branch 220 7th Street, NE. Charlottesville, VA 22901
1	Director US Army TRAC - Ft. Lee ATTN: ATRC-L, R. Cameron Fort Lee, VA 23801-6140
3	Commander US Army Materials Technology Laboratory ATTN: AMXMR-ATL SLCMT-MEC, W. Haskell SLCMT-MRD-S, K. Ofstedahl Watertown, MA 02172-0001
1	Commander US Army Strategic Defense Command ATTN: CSSD-H-MPL, Tech Lib CSSD-H-XM, Dr. Davies P.O. Box 1500 Huntsville, AL 35807
2	Commander US Army Natick Research and Development Center ATTN: AMDNA-D, Dr. D. Sieling STRNC-UE, J. Calligeros Natick, MA 01762
1	Commander US Army Engineer Division ATTN: HNDED-FD P O. Box 1500 Huntsville, AL 35807
3	Commander US Army Corps of Engineers Waterways Experiment Station ATTN: CAWES-SS-R, J. Watt CAWES-SE-R, J. Ingram CAWES-TL, Tech Lib P.O. Box 631 Vicksburg, MS 39180-0631

No of Copies	Organization
1	Commander US Army Research Office ATTN: SLCRO-D P.O. Box 12211 Research Triangle Park, NC 27709-2211
3	Commander US Army Nuclear & Chemical Agency ATTN: ACTA-NAW MONA-WE Tech. Lib. 7500 Backlick Rd, Bldg. 2073 Springfield, VA 22150
1	Director HQ, TRADOC RPD ATTN: ATRC-RPR, Mr. Radda Fort Monroe, VA 23651-5143
1	Director TRAC-WSMR ATTN: ATRC-WC, Mr. Kirby White Sands Missile Range, NM 88002-5502
1	Director TRAC-FLVN ATTN: ATRC Fort Leavenworth, KS 66027-5200
1	Commander US Army Test & Evaluation Command Nuclear Effects Laboratory ATTN: STEWS-TE-NO, Dr. J.L. Meason P.O. Box 477 White Sands Missile Range, NM 88002

No of Copies	Organization
2	Chief of Naval Operations ATTN: OP-03EG OP-985F Department of the Navy Washington, DC 20350
1	Director Strategic Systems Projects Office ATTN: NSP-43, Tech Library Department of the Navy Washington, DC 20360
1	Commander Naval Electronic Systems Command ATTN: PME 117-21A Washington, DC 20360
1	Commander Naval Facilities Engineering Command ATTN: Technical Library Washington, DC 20360
1	Commander Naval Sea Systems Command ATTN: Code SEA-62R Department of the Navy Washington, DC 20362-5101
1	Officer-in-Charge Naval Construction Battalion Center Civil Engineering Laboratory ATTN: Tech Lib Port Hueneme, CA 93041
1	Commanding Officer Naval Civil Engineering Laboratory ATTN: Code L51, J. Tancreto Port Hueneme, CA 93043-5003

No of Copies	Organization
1	Commander David Taylor Research Center ATTN: Code 522, Tech Info Ctr Bethesda, MD 20084-5000
1	Commander Naval Surface Warfare Center ATTN: Code DX-21, Library Dahlgren, VA 22448-5000
1	Officer in Charge White Oak Warfare Center Detachment ATTN: Code E232, Tech Library 10901 New Hampshire Ave Silver Spring, MD 20903-5000
1	Commanding Officer White Oak Warfare Center ATTN: Code WA501, NNPO Silver Spring, MD 20902-5000
1	Commander (Code 533) Naval Weapons Center Tech Library China Lake, CA 93555-6001
1	Commander Naval Weapons Evaluation Fac ATTN: Document Control Kirtland AFB, NM 87117
1	Commander Naval Research Laboratory ATTN: Code 2027, Tech Library Washington, DC 20375
1	Superintendent Naval Postgraduate School ATTN: Code 2124, Tech Library Monterey, CA 93940

No of Copies	Organization
2	Air Force Armament Laboratory ATTN: AFATL/DOIL AFATL/DLYV Eglin AFB, FL 32542-5000
1	AFESC/RDCS ATTN: Paul Rosengren Tyndall AFB, FL 32403
1	RADC (EMTLD/Docu Library) Griffiss AFB, NY 13441
3	Air Force Weapons Laboratory ATTN: NTE NTED NTES Kirtland AFB, NM 87117-6008
1	AFIT ATTN: Tech Lib, Bldg. 640/B Wright-Patterson AFB, OH 45433
1	FTD/NIIS Wright-Patterson AFB, OH 45433
1	U.S. Department of Energy Idaho Operations Office ATTN: Spec Programs, J. Patton 785 DOE Place Idaho Falls, ID 83402
2	Director Idaho National Engineering Laboratory EG&G Idaho Inc. ATTN: Mr. R. Guenzler, MS-3505 Mr. R. Holman, MS-3510 P.O. Box 1625 Idaho Falls, ID 83415

No of Copies	Organization
1	Director Lawrence Livermore Lab. ATTN: Tech Info Dept L-3 P.O. Box 808 Livermore, CA 94550
4	Director Los Alamos National Laboratory ATTN: Mr. Th. Dowler, MS-F602 Dr. J. Chapyak, MS-F664 Doc Control for Reports Library P.O. Box 1663 Los Alamos, NM 87545
3	Director Sandia National Laboratories ATTN: Doc Control 3141 Mr. C. Cameron, Div 6215 Mr. A. Chabai, Div 7112 P.O. Box 5800 Albuquerque, NM 87185-5800
1	Director Sandia National Laboratories Livermore Laboratory ATTN: Doc Control for Tech Library P.O. Box 969 Livermore, CA 94550
1	Director National Aeronautics and Space Administration ATTN: Scientific & Tech Info Fac P.O. Box 8757, BWI Airport Baltimore, MD 21240
1	Director NASA-Langley Research Center ATTN: Tech Lib Hampton, VA 23665
1	Director NASA-Ames Research Center Applied Computational Aerodynamics Branch ATTN: Dr. T. Holtz, MS 202-14 Moffett Field, CA 94035
2	Applied Research Associates, Inc. ATTN: N.H. Ethridge J. Keefer P.O. Box 548 Aberdeen, MD 21001
1	Aerospace Corporation ATTN: Tech Info Services P.O. Box 92957 Los Angeles, CA 90009
1	Agbabian Associates ATTN: M. Agbabian 1111 S. Arroyo Parkway, #405 Pasadena, CA 91105-3254
1	Applied Research Associates, Inc. ATTN: R. L. Guice 7114 West Jefferson Ave., Suite 305 Lakewood, CO 80235
1	Black & Veatch Engineers-Architects ATTN: H. D. Laverentz 1500 Meadow Lake Parkway Kansas City, MO 64114
1	The Boeing Company ATTN: Aerospace Library P.O. Box 3707 Seattle, WA 98124
1	California Research & Technology, Inc. ATTN: M. Rosenblatt 20943 Devonshire Street Chatsworth, CA 91311

No of Copies	Organization
1	Carpenter Research Corporation ATTN: H. Jerry Carpenter 27520 Hawthorne Blvd., Suite 263 P.O. Box 2490 Rolling Hills Estates, CA 90274
1	Dynamics Technology, Inc. ATTN: D. T. Hove Suite 300 21311 Hawthorne Blvd. Torrance, CA 90503
1	EATON Corporation Defense Valve & Actuator Div. ATTN: Mr. J. Wada 2338 Alaska Ave. El Segundo, CA 90245-4896
2	FMC Corporation Advanced Systems Center ATTN: Mr. J. Drotleff Ms. C. Krebs, MDP95 2890 De La Cruz Boulevard Box 58123 Santa Clara, CA 95052
1	Goodyear Aerospace Corporation ATTN: R. M. Brown, Bldg 1 Shelter Engineering Litchfield Park, AZ 85340
4	Kaman AviDyne ATTN: Dr. R. Ruetenik (2 cys) Mr. S. Criscione Mr. R. Milligan 83 Second Avenue Northwest Industrial Park Burlington, MA 01830

No of Copies	Organization
3	Kaman Sciences Corporation ATTN: Library P. A. Ellis F. H. Shelton 1500 Garden of the Gods Road Colorado Springs, CO 80907
1	Kaman Sciences Corporation ATTN: Mr. F. W. Balicki 6400 Uptown Boulevard N.E. Suite 300 Albuquerque, NM 87110
2	Kaman-TEMPO ATTN: DASIAC Don Sachs P.O. Drawer QQ 816 State Street Santa Barbara, CA 93102
1	Ktech Corporation ATTN: Dr. E. Gaffney 901 Pennsylvania Avenue, N.E. Albuquerque, NM 87111
1	Lockheed Missiles & Space Co. ATTN: J. J. Murphy, Dept. 81-11, Bldg. 154 P.O. Box 504 Sunnyvale, CA 94086
2	McDonnell Douglas Astronautics Corporation ATTN: Robert W. Halprin K.A. Heinly 5301 Bolsa Avenue Huntington Beach, CA 92647
1	Orlando Technology, Inc. ATTN: Mr. D. Matuska P.O. Box 855 Shalimar, FL 32579

No of Copies	Organization
2	Physics International Corporation 2700 Merced Street San Leandro, CA 94577
2	R&D Associates ATTN: Technical Library Dr. Allan Kuhl P.O. Box 9695 Marina Del Rey, CA 90291
1	R&D Associates ATTN: G.P. Ganong P.O. Box 9377 Albuquerque, NM 87119
2	Science Applications, Inc. ATTN: W. Layson John Cockayne P.O. Box 1303 1710 Goodridge Drive McLean, VA 22102
1	Science Applications International Corp. ATTN: Mr. J. Guest 2301 Yale Blvd. SE Suite E Albuquerque, NM 87106
1	Sparta, Inc. Los Angeles Operations ATTN: I. B. Osofsky 3440 Carson Street Torrance, CA 90503
1	Sunburst Recovery, Inc. ATTN: Dr. C. Young P.O. Box 2129 Steamboat Springs, CO 80477
1	Sverdrup Technology, Inc. ATTN: R. F. Starr P.O. Box 884 Tullahoma, TN 37388

No of Copies	Organization
3	SRI International ATTN: Dr. G. R. Abrahamson Dr. J. Gran Dr. B. Holmes 333 Ravenswood Avenue Menlo Park, CA 94025
2	S-CUBED A Division of Maxwell Laboratories, Inc. ATTN: C. E. Needham Dr. Lynn Kennedy 2501 Yale Blvd., SE Albuquerque, NM 87106
3	S-CUBED A Division of Maxwell Laboratories, Inc. ATTN: Technical Library R. Duff K. Pyatt PO Box 1620 La Jolla, CA 92037-1620
1	Texas Engineering Experiment Station ATTN: Dr. D. Anderson 301 Engineering Research Center College Station, TX 77843
1	Thermal Science, Inc. ATTN: R. Feldman 2200 Cassens Dr. St. Louis, MO 63026
1	TRW Ballistic Missile Division ATTN: H. Korman, Mail Station 526/614 P.O. Box 1310 San Bernadino, CA 92402

No of Copies	Organization
1	Battelle ATTN: TACTEC Library, J. N. Higgins 505 King Avenue Columbus, OH 43201
1	California Institute of Technology ATTN: T. J. Ahrens 1201 E. California Blvd. Pasadena, CA 91109
2	Denver Research Institute ATTN: Mr. J. Wisotski Technical Library P.O. Box 10758 Denver, CO 80210
1	Massachusetts Institute of Technology Aeroelastic and Structures Research Laboratory ATTN: Dr. E. A. Witmer Cambridge, MA 02139
1	Massachusetts Institute of Technology ATTN: Technical Library Cambridge, MA 02139
2	New Mexico Engineering Research Institute (CERF) University of New Mexico ATTN: Dr. J. Leigh Dr. R. Newell P.O. Box 25 Albuquerque, NM 87131
1	Northrop University ATTN: Dr. F. B. Safford 5800 W. Arbor Vitae St. Los Angeles, CA 90045
4	Southwest Research Institute ATTN: Dr. W. E. Baker A. B. Wenzel Dr. C. Anderson S. Mullin 6220 Culebra Road San Antonio, TX 78284
1	Stanford University ATTN: Dr. D. Bershader Durand Laboratory Stanford, CA 94305
3	University of Maryland Department of Mechanical Engineering ATTN: Dr. W. Fourney Dr. R. Dick Dr. J. Williams College Park, MD 20742
Aberdeen Proving Ground	
1	Cdr, USATECOM ATTN: AMSTE-TE-F, L. Teletski
1	Cdr, USATHMA ATTN: AMXTH-TE

INTENTIONALLY LEFT BLANK.